crystals

MDPI

Article

Intermolecular Bonding Interactions Within Acenaphthene *Peri*-Diselenide Radical Cations: Combining Chalcogen Bonding and Pancake Bonding

Hrudya Pariyacheri Padikkal [1], Olivier Jeannin [1], Nicolas Quéméré [1], Ie-Rang Jeon [2,*] and Marc Fourmigué [1,*]

[1] Institut des Sciences Chimiques de Rennes, CNRS-UMR 6226, Université de Rennes, 35042 Rennes, France; hrudya.pariyacheri@univ-rennes.fr (H.P.P.); olivier.jeannin@univ-rennes.fr (O.J.); nicolas.quemere@univ-rennes.fr (N.Q.)

[2] Centre de Recherche Paul Pascal, CNRS-UMR 5031, UMR 5031, Université de Bordeaux, 33600 Pessac, France

* Correspondence: ie-rang.jeon@u-bordeaux.fr (I.-R.J.); marc.fourmigue@univ-rennes.fr (M.F.)

Abstract

Cyclic 1,2-diselenides are known to exhibit three σ-holes around the Se atoms—two in the prolongation of the Se–Se bond and one merging the two electron-depleted areas in the prolongation of the C–Se bonds. Among them, naphthalene *peri*-diselenides were recently isolated in their radical cation form with halometallates, affording 1:1 salts, where charge activation upon oxidation leads to strong Se•••Cl/Br chalcogen bond (ChB) interactions. Acenaphthene *peri*-diselenide (**1**) is shown here to be readily oxidized to its cation radical, showing various association modes of the $\mathbf{1}^{+\bullet}$ species in the solid state. When engaged in electrocrystallization experiments with $(Bu_4N)(FeCl_4)$, acenaphthene *peri*-diselenide (**1**) afforded two salts of the radical cation, formulated as $(\mathbf{1})_2(Fe_2Cl_6O)$ and $(\mathbf{1})(FeCl_4)$, depending on the electrocrystallization conditions. In both salts, short and highly directional Se•••Cl chalcogen bond (ChB) interactions take place, simultaneously involving all three σ-holes surrounding the diselenide bridge, with the reduction ratio (relative to the van der Waals Se•••Cl contact distance of 1.90 + 1.75 = 3.65 Å) reduced to 0.89. In addition, while cation radicals in $(\mathbf{1})_2(Fe_2Cl_6O)$ adopt head-to-tail alternated stacks without any intermolecular Se•••Se contacts, they organize in $(\mathbf{1})FeCl_4$ into twisted-cofacial dimers, with an intra-dimer Se•••Se contact as short as 3.197(2) Å, i.e., a reduction ratio of 0.84. Such structural organization is reminiscent of those observed in dithiadiazolyl/diselenadiazolyl radicals, which associate into dimers, most often in a *cis*-cofacial geometry. Here, the $\mathbf{1}^{+\bullet}$ radicals adopt either a head-to-tail (*trans*-cofacial) geometry (in the $Fe_2Cl_6O^{2-}$ salt) or a distorted twisted-cofacial geometry (in the $FeCl_4^-$ salt), further stabilized by the chelating $FeCl_4^-$.

Keywords: diselenides; chalcogen bonding; pancake bonding; ion radical salt

Check for updates

Academic Editor: Ana M. Garcia-Deibe

Received: 20 July 2026
Revised: 17 August 2026
Accepted: 19 August 2026
Published: 26 August 2026

Copyright: © 2026 by the authors. Licensee MDPI, Basel, Switzerland. This article is an open access article distributed under the terms and conditions of the Creative Commons Attribution (CC BY) license.

1. Introduction

The solid-state chemistry of π-type radicals is based on a combination of (i) intermolecular interactions found in any molecular solid such as van der Waals interactions, π–π interactions, and hydrogen/halogen/chalcogen bonding interactions [1] and (ii) overlap interactions of the SOMO of such open-shell species, also known as pancake bonding [2,3]. The outcome of such combined interactions governs their solid-state organization, and, as a consequence, their conducting and magnetic properties. Furthermore, the overlap interactions of the SOMO of open-shell π-type radicals can take many different forms,

(i) non- or very weakly interacting species; (ii) localized σ-bonding between two atoms of the two interacting radicals; (iii) face-to-face multicenter association of the π-type SOMO into strongly dimerized, isolated systems (pancake bonding) [4–7]; and (iv) delocalized bonding interactions within a (partially) filled conduction band [3].

Among π-type radicals, cationic species, such as those derived from tetrathiafulvalene (TTF) derivatives, occupy a large space in this landscape, as (i) they can crystallize into mixed-valence, highly conducting salts [8] and (ii) oxidation to the radical cation state activates the TTF substituents, enabling enhanced additional supramolecular interactions through stronger hydrogen, halogen or chalcogen bonding. This has been revealed through substitution of the TTF core with halogens (I, Br) [9–12] or, more recently, with selenomethyl (SeMe) moieties [13–15], as the oxidation of the TTF strongly reinforces the σ-hole in the prolongation of the C_{TTF}–I or C_{TTF}–Se bond, with interactions with the counter ion (Cl^-, Br^-, ClO_4^-, $TCNQF_n^-$, . . .) acting as the Lewis base. We have recently re-explored another family of redox active electron-rich donor molecules able to oxidize into cation radicals, namely derivatives of naphthalene selenides, as illustrated in Scheme 1. Naphthalene *tetraselenide* **3** and tetracene *tetraselenide* **4** have been known, for more than forty years, to afford cation radical salts upon oxidation [16,17] and, further, are blessed with the setting of intermolecular interactions involving Se atoms as chalcogen bond (ChB) donors and counter ions as Lewis bases. Such ChB interactions are found in the Cl^- salts of **3** and **4** [16,17] but also in charge transfer complexes with TCNQ as the acceptor with the setting of Se●●●N ChB interactions [18].

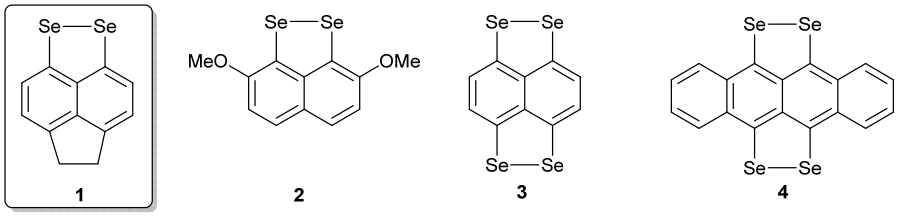

Scheme 1. Molecular structures of investigated di- and tetraselenides.

Concerning the chalcogen bond donor ability of such derivatives, it has been demonstrated that the four σ-holes usually observed in the prolongation of the covalent bonds to a given divalent Se atom in acyclic diselenides (Scheme 2a) [19–21] transform within cyclic 1,2-diselenole motifs [22] into a set of only three electron-depleted areas in the rigid heterocycle, from the merging of the two σ-holes in the prolongation of the C–Se bonds (Scheme 2b,c). Such effects were analyzed in detail in 3H-1,2-benzodiselenol-3-(thi)one and sulfur analogs (Scheme 2b) [23], demonstrating that each chalcogen bond (ChB) involves a σ-hole region and shows a charge-depleted (CD)●●●charge-concentrated (CC) interaction that aligns with the internuclear direction of the atoms to which the CD and CC sites belong. The alignment holds simultaneously for all of the ChB interactions in each crystal structure, indicating that CD●●●CC interactions drive molecular orientation in molecular assembly.

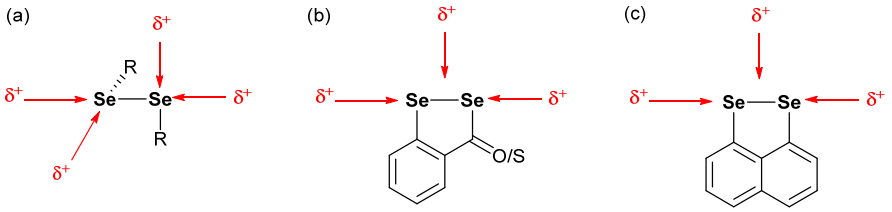

Scheme 2. Charge-depleted area (indicated by red arrows) on selenium atoms in (**a**) acyclic diselenides, (**b**) and (**c**) cyclic diselenides.

On these bases, we reported recently that the dimethoxy-substituted naphthalene *diselenide* derivative **2** (Scheme 1), more difficult to oxidize than the tetraselenides and known to form a neutral charge transfer complex with TCNQ [24], could be also successfully oxidized to the cation radical and co-crystallized with halometallates as a counter ion [25]. In these 1:1 salts, head-to-tail stacking of the radicals led to the formation of dimerized chains, further associated through strong Se●●●Cl/Br ChB interactions involving the three σ-holes surrounding the diselenide bridge. We want to extend here this approach to another *diselenide*, namely acenaphthene *peri*-diselenide **1** (Scheme 1), considering that the ethylenic bridge in a *peri* position will also impart in **1**, as the methoxy groups in **2**, an electron-rich character favoring the stabilization of its cation radical. Additionally, it is also hoped that the absence of the two methoxy groups present in **2** might allow for stronger ChB interactions involving the two σ-holes in the prolongation of the Se–Se bonds, as they were partially hidden in the salts of **2**. We report here the preparation, crystal structure and electronic properties of **1**, together with two cation radical salts blessed with very different solid-state organization of the radical species but recurrent, strong Se●●●Cl ChB interactions.

2. Experimental Section

2.1. Syntheses

2.1.1. Synthesis of Acenaphthene Diselenide **1**

In a 500 mL oven-dried round bottom flask, 1,2-dibromo-5,6-dihydroacenaphthene [26] (2.62 g, 8.4 mmol, 1 eq.) and tetramethylethylenediamine (2.5 mL, 16.8 mmol, 2 eq.) were dissolved in 200 mL of dry ether. The mixture was cooled to −78 °C. A solution of *n*-butyllithium (1.6 M in hexanes, 6.3 mL, 10.08 mmol, 1.2 eq.) was added dropwise. The mixture was then stirred for 15 min. Further, elemental selenium (0.8 g, 10.08 mmol, 1.2 eq.) was added, and the mixture was stirred at −40 °C for 2 h. The mixture was cooled again to −78 °C. A second addition of *n*-butyllithium, followed by stirring for 15 mn and selenium addition, was carried out as in the previous step. The mixture was then stirred at −40 °C for 90 mn. After warming up to room temperature, acetic acid (2 mL, 33.59 mmol, 4 eq.) was added and a stream of compressed air was bubbled for 24 h. The solution was evaporated to dryness using a rotary evaporator and the residue was dissolved in DCM. The organic phase was washed twice with water. The aqueous phase was again extracted with DCM. The pure compound 0.8 g (30%) was obtained after column chromatography (petroleum ether: ethyl acetate, 9:1), and recrystallization from toluene. Mp: 200.6 °C (lit. [27] Mp.:198–200 °C); ^{1}H NMR (400 MHz, $CDCl_3$) δ 7.23 (d, *J* = 7.3 Hz, 2 H), 7.07 (dt, *J* = 7.5, 0.8 Hz, 2H), 4.02 (d, 0.9 Hz, 4H); ^{13}C NMR (400 MHz, $CDCl_3$) δ 142.0 121.6, 121.1, 30.3; ^{77}Se NMR (400 MHz, $CDCl_3$): δ 461. Elem. Anal. Calcd. for $C_{12}H_8Se_2$: C, 46.47; H, 2.60; found: C, 46.92; H, 2.60.

2.1.2. Electrocrystallization Experiments

In an H-shaped cell, **1** (7 mg) was added and the cell was flushed with Ar (*n*-Bu_4N)$FeCl_4$ (100 mg) which was dried under vacuum overnight and dissolved in anhydrous 1,2-dichloroethane (10 mL), and the solution was added slowly to the cell containing the donor **1**. The cell was equipped with platinum electrodes (length 1.5 cm, diameter 1 mm) and used in a galvanostatic mode with a constant current of 3 μA, at a controlled temperature (20 ± 2 °C), under Ar. The salt was obtained as long black needles on the electrode within 1 week. The reproducibility was checked from several electrocrystallization batches, needed to collect enough samples to perform the magnetic measurements (10 mg), as discussed below. Performing the experiments in air (rather than under Ar) afforded a different salt, formulated as $(\mathbf{1})_2(Fe_2Cl_6O)$, which was obtained on several occasions.

2.2. X-Ray Crystallography

Single crystals that were suitable for X-ray analysis were coated with Paratone-N oil (Hampton Research, Aliso Viejo, CA, USA) and mounted on a MicroMountsTM rod (MiTeGem, Ithaca, NY, USA). X-ray diffraction measurements were performed on a APEX-II diffractometer (Bruker, Karlsruhe, Germany) operating with a Mo Kα (λ = 0.71073 Å) X-ray tube with a graphite monochromator. Structures were solved by a dual-space algorithm using SHELXT-2018/2 [28] and then refined with full-matrix least-square methods based on F^2 (SHELXL-2025/1) [29] with the aid of the WINGX-2026-1 program [30]. All non-hydrogen atoms were refined with anisotropic atomic displacement parameters. H atoms were finally included in their calculated positions. A summary of the crystallographic data and the structure refinement is given in Table S1. CCDC 2574025-2574027 contains the supplementary crystallographic data for **1**, (**1**)$_2$(Fe_2Cl_6O) and (**1**)$FeCl_4$ respectively. These data can be obtained free of charge via http://www.ccdc.cam.ac.uk/conts/retrieving.html (accessed on 18 August 2026) (or from the CCDC, 12 Union Road, Cambridge CB2 1EZ, UK; Fax: +44 1223 336033; E-mail: deposit@ccdc.cam.ac.uk).

2.3. Magnetic Measurements

The magnetic measurements were carried out with a MPMS-XL SQUID magnetometer (Quantum Design, San Diego, CA, USA) working between 1.85 and 400 K with applied static fields (H) ranging from -7 to 7 T. The data were collected on polycrystalline samples of (**1**)($FeCl_4$), sealed in a polypropylene bag (size $\approx 1 \times 0.5 \times 0.02$ cm; 10.04 mg). The resulting data were corrected for the sample holder and intrinsic diamagnetic contributions of the sample. A M vs. H measurement was performed at 100 K to confirm the absence of ferromagnetic impurities (Figure S1) (see Supplementary Materials).

2.4. Theoretical Calculations

Geometry optimization and vibrational frequency calculations were performed with density functional theory (DFT) [31,32] using the hybrid Becke-3 parameter exchange functional [33,34] and the Lee–Yang–Parr non-local correlation functional [35] (B3LYP) implemented in the Gaussian 16 program suite [36], using the def2-tzvp basis set, GD3BJ dispersion correction [37] and the default convergence criterion implemented in the program. Determination of the $V_{S,max}$ and spin density on each atom was done using the Multiwfn3.8 program [38,39], and figures (molecular structure, ESP and spin density maps) were generated using GaussView 6.0.16. Isovalues of 0.001, 0.004 and 0.04 u.a. were used for ESP, spin density and MO's maps, respectively.

3. Results and Discussion

3.1. Synthesis and Molecular Properties

Preparation of **1** was performed following reported procedures, as already described by Aso et al. and Benson et al. (Scheme 3) [27,40]. It is based on the bromination of acenaphthene in *peri* positions, followed by Li-bromine exchange, selenation and aerial oxidation to the diselenide **1**. Cyclic voltammetry experiments performed in CH_2Cl_2 solution with (Bu_4N)(PF_6) 0.1 M as supporting electrolyte at a scan rate of 100 mV/s on a Pt working electrode (Figure S2) confirm the electron-donor character of the molecule with a first oxidation wave found at +0.68 V vs. SCE, in line with the reported value of +0.57 V vs. Ag/AgCl in CH_2Cl_2 0.1 M (Bu_4N)(ClO_4) on a glassy-carbon working electrode [40].

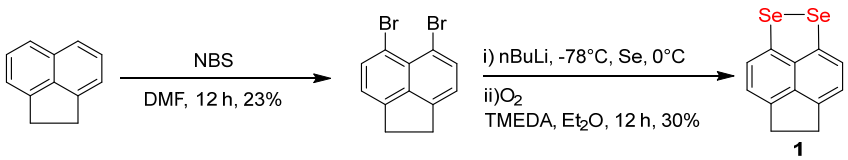

Scheme 3. Synthetic procedure to **1**.

The X-ray crystal structure of neutral **1** has already been reported [27], but the limited precision on intramolecular bond lengths led us to re-analyze the compound, which crystalizes in the monoclinic system, space group $P2_1/n$, with two crystallographically independent molecules in the unit cell. As shown in Figure 1, chalcogen bond interactions are clearly identified, with atoms Se3 and Se4 acting as ChB donors toward the lone pairs of Se1 and Se2, with intermolecular distances at 3.565(2), 3.658(1) and 3.730(1) Å, i.e., a reduction ratio (RR, relative to van der Waals contact distance) of 0.94, 0.96 and 0.98. Additionally, short Se1●●●Se3 contacts (3.424(5)Å, RR = 0.90) are also noticed. This tetrameric motif interacts only weakly with neighboring ones through weaker Se4●●●Se4 contacts at a van der Waals contact distance (3.811(1) Å).

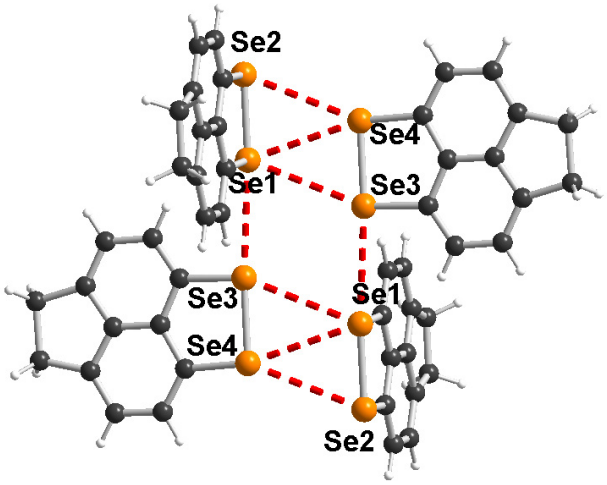

Figure 1. Detail of the Se●●●Se interactions (red dotted lines) in the crystal structure of **1**. See text for detailed Se●●●Se distances and Figure S3 for a view of the unit cell. C atoms are in black, Se atoms in orange and H atoms in white.

3.2. Electronic Structures and Electrocrystallizations

As deduced from DFT calculations, the distribution of the HOMO of **1** and that of the spin density in $\mathbf{1}^{+\bullet}$ are shown in Figure 2a,b. Both are mostly concentrated on the Se atoms of the peripheral diselenide bridge, with limited delocalization on the other C atoms, and a node in the HOMO on the two carbon atoms fusing the six-membered cycles. The ESP maps of the neutral and cation radical species of the donor are depicted in Figure 2c,d. The electrostatic potential surface calculations of the cation radical $\mathbf{1}^{+\bullet}$ reveal that the σ-holes lie in the molecular plane, with a total of three σ-holes on the Se atoms: two in the prolongation of the Se–Se bond and one perpendicular to this Se–Se bond, corresponding to the convergence of the two individual σ-holes along the C–Se bonds. The potentials ($V_{s,max}$) on the σ-holes in the prolongation of the Se–Se bond increase from 19.10 kcal mol^{-1} in the neutral state to 108.24 kcal mol^{-1} in the cation radical state. Also, the amplitude of $V_{s,max}$ of the σ-hole orthogonal to the Se–Se bond enhances drastically from 16.74 kcal mol^{-1} in neutral donor to 106.52 kcal mol^{-1} in the cation radical. Based on these results, it is expected that ChB interactions will be strongly activated in cation radical salts, favoring interactions with the counterions. Thus, the three σ-holes exhibit similar and (strong) amplitude, at

variance with previous results reported for the dimethoxynaphthalene diselenidene **2** (see Scheme 1), where the amplitude of two σ-holes in the prolongation of the Se–Se bond was lowered down to 80 kcal mol^{-1}, a consequence of the electron-releasing effect of the neighboring methoxy groups.

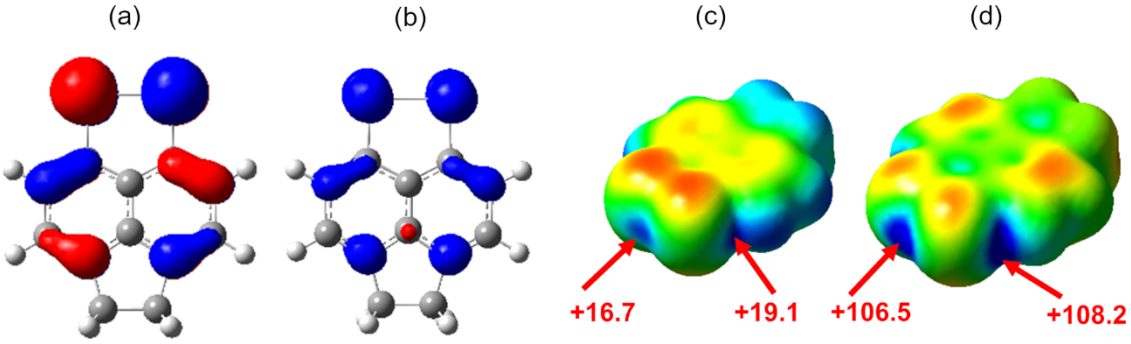

Figure 2. Calculated electronic properties of **1** with (**a**) HOMO of **1**, (**b**) spin density distribution in **1**$^{+\bullet}$, ESP map in **1**, and (**d**) ESP map in **1**$^{+\bullet}$. Isovalues of 0.04, 0.004 and 0.001 u.a. were used for HOMO, spin density and ESP maps respectively. The electropositive regions of $V_{s,max}$ are represented in (**c**) and (**d**) in blue and the electronegative surfaces in red, with a color scale in the range +/−18.8 kcal mol^{-1} for neutral **1** and in the range +70.0/+100.4 kcal mol^{-1} for cationic **1**$^{+\bullet}$. Numerical values refer to the positive extrema of $V_{s,max}$ (in kcal mol^{-1}). Visible C and H atoms are in dark and light grey respectively.

Electrocrystallization experiments were performed with the $FeCl_4^-$ anion and its diamagnetic analog $GaCl_4^-$, both as Bu_4N^+ salts. The technique is based on the precipitation/crystallization at the anode, under adapted conditions of solvent/temperature/current, of the generated cation radical salt with the anion of the electrolyte, while the Bu_4N^+ cation is reduced at the cathode [41]. Despite our efforts, we were not able to grow crystals for X-ray structure determination with $(Bu_4N)(GaCl_4)$ as electrolyte. The generated radicals diffused in the solution which turned dark but no crystals were obtained. Lowering the temperature or increasing the current led to non-crystalline material. This might be due to the slightly smaller size of this anion when compared with $FeCl_4^-$, possibly giving rise to more soluble phases which did not crystallize on the anode. In the corresponding salts of the dimethoxynaphthalene diselenide **2** (Cf Scheme 1) reported earlier, this effect was found to also provide $GaCl_4^-$ salts with difficulties and affected with a notable positional disorder [25]. On the other hand, electrocrystallization experiments with $(Bu_4N)(FeCl_4)$ afforded a 1:1 salt, formulated as (**1**)$FeCl_4$. In some instances where the electrocrystallization cell was not tight enough, introduction of air (and probably water) in the experiments afforded an unexpected phase incorporating the dianionic dinuclear species, namely $(Fe_2Cl_6O)^{2-}$, and formulated as $(\mathbf{1})_2(Fe_2Cl_6O)$, as deduced from the X-ray crystal structure resolution (See below). This transformation of the $FeCl_4^-$ anion is not unknown and has been reported in several instances from its hydrolysis [42–44] or its treatment with sodium trimethylsiloxide [45]. It has also been observed in the electrocrystallization of tetrathiafulvalene derivatives using an undoped (100)-oriented silicon wafer as electrode where the SiO_2 present at the electrode surface might have played a similar role [46].

Nevertheless, the obtention of these two salts demonstrates that the isolation of cation radical salts of **1** is achievable, at variance with the only reported results of this family of donors where *neutral* charge transfer complexes with TCNQ were isolated [40]. It also gives the opportunity to evaluate how the oxidation of the radical cation modifies the electrostatic surface distribution, and particularly the localization and amplitude of the σ-holes on the Se atoms, toward specific ChB interactions.

3.3. Cation Radical Salt with $Fe_2Cl_6O^{2-}$

The $Fe_2Cl_6O^{2-}$ salt crystallizes in the triclinic system, space group $P\bar{1}$, with one radical cation in general position, and the oxygen atom of the $Fe_2Cl_6O^{2-}$ dianion on an inversion center, giving a linear Fe–O–Fe geometry and a staggered conformation of the two $FeCl_3$ moieties (Figure 3a). This geometry contrasts with most examples of this μ-oxo-bridged dinuclear iron complex which most often show a bent geometry [47,48].

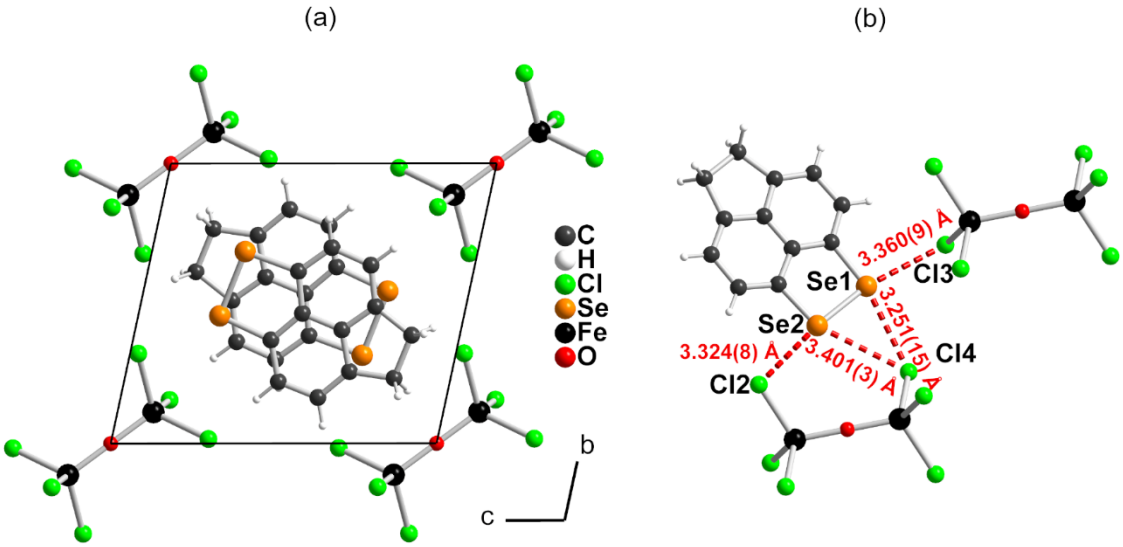

Figure 3. (**a**) Projection view of the unit cell along *a*, and (**b**) details of the Se●●●Cl ChB interactions (red dotted lines).

An evolution in the intramolecular bond distances in the donor has been observed, moving from the neutral state to the cation radical (Table 1). Upon oxidation, the Se–Se bond (a) and the C–Se and C–C bonds (b) and (e) that are antibonding in nature in the HOMO (Figure 2a) show a decrease of their intramolecular distances (−2.1, −1.6, −0.45%) while the C–C bond (d), which is bonding in nature in the HOMO, increases by +1.6%, and the non-bonding C–C bond (c) preserves its nature, since one of the carbon atoms is present on the node.

Table 1. Evolution of averaged bond lengths (in Å) within **1** and its cation radicals.

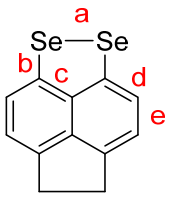

	a	b	c	d	e
Neutral 1	**2.373**	**1.911**	**1.411**	**1.375**	**1.419**
(1)$_2$(Fe$_2$OCl$_6$)	**2.325**	**1.876**	**1.403**	**1.394**	**1.415**
(1)(FeCl$_4$)	**2.319**	**1.884**	**1.404**	**1.402**	**1.408**

In the solid state, the radical cations stack along the *a* axis (Figure 3a). The presence of the inversion centers gives rise to two different interplanar distances (Figure 4a) and overlap patterns. As shown in Figure 4b, the short, intra-dimer, plane-to-plane distance is associated with a perfect head-to-tail overlap, while a shifted inter-dimer overlap (Figure 4c) is found with a larger plane-to-plane distance. This solid-state organization of a strongly

dimerized spin chain allows us to anticipate an essentially nil contribution of the cations to the magnetic response of this salt (see below), as already observed, for example, in (**2**)$FeCl_4$ [25]. The radical chains are surrounded by the $Fe_2Cl_6O^{2-}$ anions through short and directional ChB interactions involving the Se atoms as ChB donors and the Cl atoms as ChB acceptors. Indeed, as shown in Figure 3b, each of the three crystallographically independent chlorine atoms (Cl2, Cl3 and Cl4) is located essentially in the molecular plane of $\mathbf{1}^{+\bullet}$ and is engaged in a short and highly directional Se•••Cl ChB interaction (Table 2), pointing precisely toward the extrema of the ESP of the cation. The four Se•••Cl bond distances are found in the range 3.25–3.40 Å, corresponding to very small RR values, from 0.89 to 0.93, and demonstrating the efficiency of the interaction.

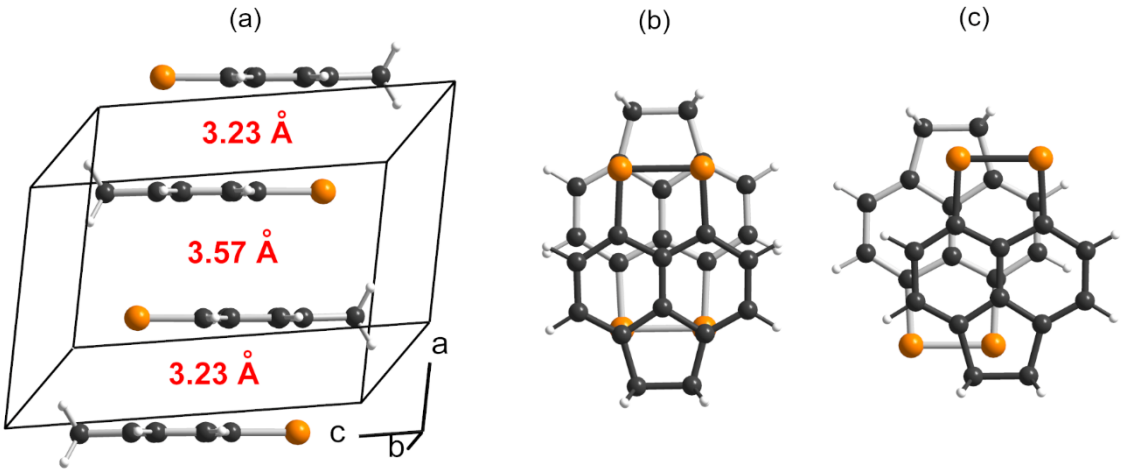

Figure 4. Solid-state organization within (**1**)$_2Fe_2Cl_6O$, with (**a**) a view of the dimerized stack, (**b**,**c**) the two different intra- and inter-dimer overlap patterns associated with, respectively, the short (3.23 Å) and the large (3.57 Å) plane-to-plane distances.

Table 2. Structural characteristics of the Se•••Cl ChB in (**1**)$_2(Fe_2OCl_6)$. The Se atom acting as ChB donor is highlighted in bold. See Figure 3b for atom numbering.

Se•••Cl Interaction	Se•••Cl Dist. (Å)	RR	(X–)Se•••Cl Angle (°)
(Se2–)**Se1**•••Cl3	3.360(9)	0.92	170.08(4)
(C1–)**Se1**•••Cl4	3.251(15)	0.89	165.4(2)
(Se1–)**Se2**•••Cl2	3.324(8)	0.91	170.04(4)
(C7–)**Se2**•••Cl4	3.401(3)	0.93	158.7(2)

3.4. Cation Radical Salt with $FeCl_4^-$

(**1**)$FeCl_4$ crystallizes in the monoclinic system, space group $P2_1/c$. The asymmetric unit is composed of two independent $\mathbf{1}^{+\bullet}$ radical cations associated with two independent $FeCl_4^-$ anions, all of them in general position, hence the 1:1 stoichiometry. As shown in Figure 5a, the cations stack along the *a* axis and are surrounded by $FeCl_4^-$ anions, fully isolating the organic stacks from one another. The interactions between radicals are here completely different: they stack in distorted eclipsed conformation associated with two very different intermolecular Se•••Se distances, one found at the remarkably short distance at 3.197(2) Å, i.e., an RR value at 0.84, and one found at 3.867(2) Å, well above the van der Waals contact distance (3.80 Å), allowing us to consider that the dimers are essentially isolated from each other.

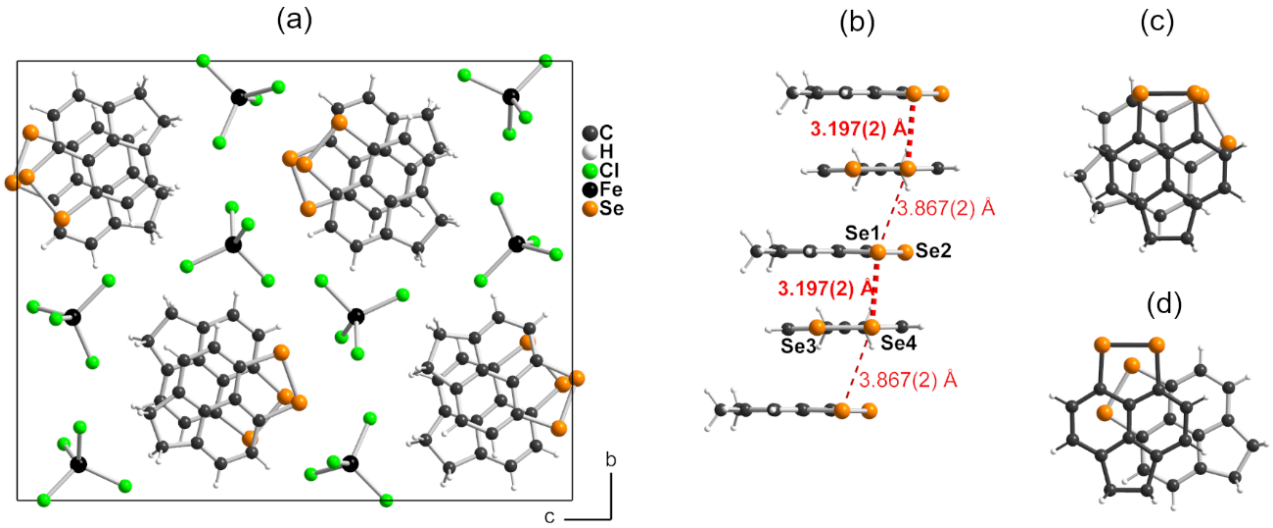

Figure 5. Structure of (**1**)$FeCl_4$ with (**a**) projection of the unit cell along the *a* axis, (**b**) lateral view of the organic stack, showing the strong dimerization through one short Se•••Se contact at 3.197(2) Å, (**c**) detail of the intra-dimer overlap with essentially superposed Se atoms and (**d**) detail of the inter-dimer overlap.

Specific Se•••Cl ChB interactions take place in (**1**)$FeCl_4$ (Figure 6a) with the three σ-holes of each cation radical engaged in short interactions and RR values down to 0.88 (Table 3). As shown in Figure 6b, two $FeCl_4^-$ anions (highlighted with black Fe–Cl bonds) play the role of a pincer to further strengthen the dimer association by interaction with the σ-holes of two different radicals. Those ChB interactions are notably shorter than those reported earlier in the dimethoxynaphthalene diselenide salt (**2**)$FeCl_4$ [25], where the two methoxy groups, located α to the diselenide bridge, essentially hindered the approach of Cl atoms toward the two σ-holes in the prolongation of the Se–Se bond.

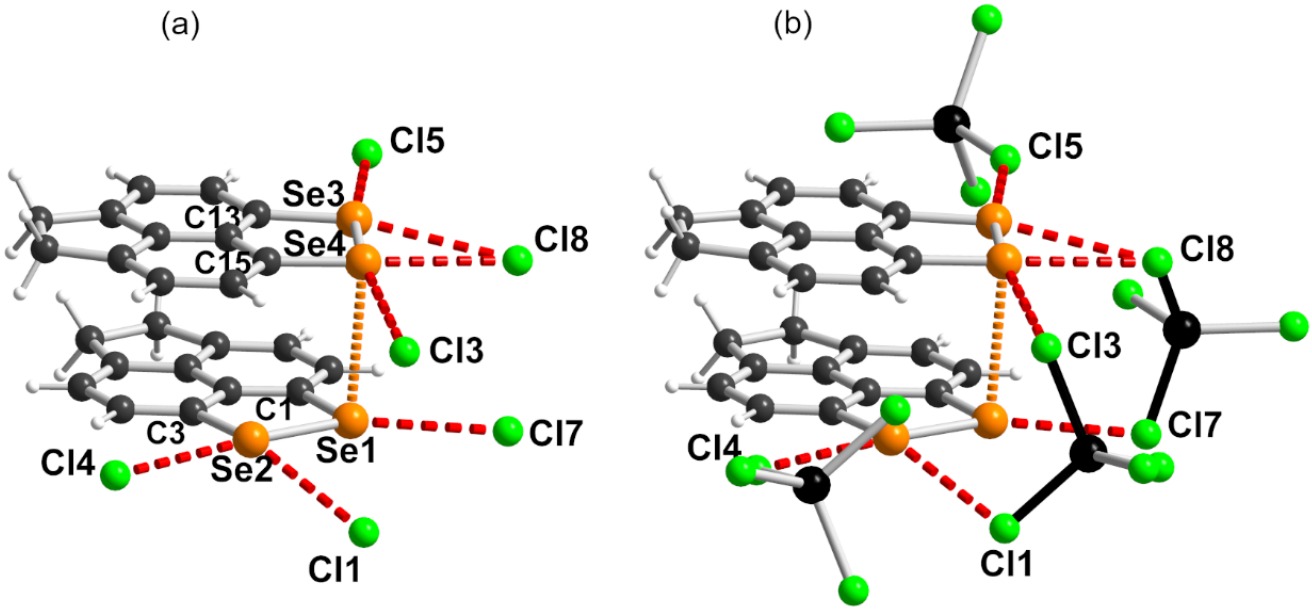

Figure 6. Detail of the Se•••Cl (red dotted lines) ChB interactions in (1)$FeCl_4$ showing (**a**) the six chlorine atoms facing the σ-holes on Se atoms in the two independent cations, and (**b**) the pincer role played by the $FeCl_4^-$ to link together the two cations.

Table 3. Structural characteristics of the Se●●●Cl ChB interactions in (**1**)$FeCl_4$. The Se atom acting as ChB donor is highlighted in bold. See Figure 6a for atom numbering.

Se●●●Cl Interaction	Se●●●Cl Dist. (Å)	RR	(X–)Se●●●Cl Angle (°)
(Se2–)Se1●●●Cl7	**3.550(3)**	**0.97**	**167.44(2)**
(Se1–)Se2●●●Cl4	**3.295(1)**	**0.90**	**176.10(2)**
(C3–)Se2●●●Cl1	**3.429(6)**	**0.94**	**162.56(9)**
(Se4–)Se3●●●Cl5	**3.209(1)**	**0.88**	**170.80(2)**
(C13–)Se3●●●Cl8	**3.373(4)**	**0.92**	**159.29(8)**
(Se3–)Se4●●●Cl3	**3.233(3)**	**0.88**	**163.84(2)**
(C15–)Se4●●●Cl8	**3.262(2)**	**0.89**	**163.91(9)**

3.5. Magnetic Properties

As mentioned above, (**1**)$_2$(Fe_2OCl_6) was obtained in very limited quantities, hindering its characterization by magnetic measurements. We can still anticipate a non-magnetic behavior of the head-to-tail dicationic dimers while the magnetic contribution of the bimetallic $(Fe_2Cl_6O)^{2-}$ species has been reported to follow a dimer model associated with antiferromagnetic interactions between the two Fe^{III} magnetic centers [42,43]. On the other hand, the magnetic properties of (**1**)$FeCl_4$ were analyzed by SQUID magnetometry on polycrystalline samples. As mentioned above, the association of the cation radicals through one very short Se●●●Se bond leaves the organic part magnetically silent and the sole magnetic contribution stems from the $FeCl_4^-$ moieties. Preliminary investigation of the magnetization as a function of applied field at 100 K shows a linear dependance indicative of the absence of ferromagnetic impurities (Figure S3). Temperature dependence of the magnetic susceptibility was determined on a polycrystalline sample and the resulting plot of χT vs. T is shown in Figure 7. At 300 K, the χT value is 3.786 cm^3 K mol^{-1}, a value slightly lower than that expected for a high-spin $S = 5/2$ Fe^{III} ion (C = 4.375 cm^3 K mol^{-1} with $g = 2$). It might indicate the presence of non-magnetic impurities (trapped solvent) or sample degradation. The χT product gradually decreases upon lowering the temperature, indicating the presence of predominant antiferromagnetic interactions between the Fe^{III} spins, with a θ value of −13.24 K, as deduced from the Curie–Weiss fit of χ^{-1} vs. T applied in the 30–300K range (Figure 7 inset).

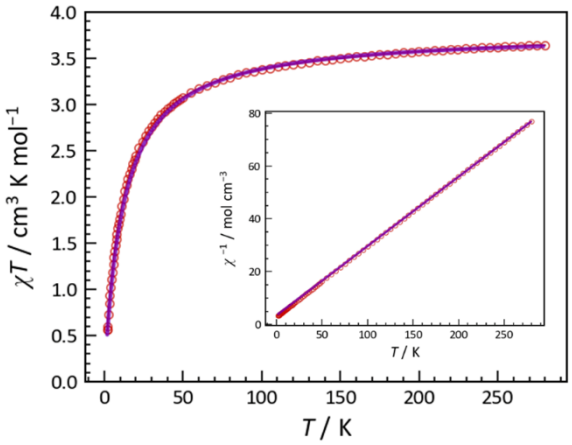

Figure 7. Temperature dependence of the χT product measured at 0.1 T for (**1**)$FeCl_4$. In inset: Temperature dependence of χ^{-1}. The solid pink lines are the best fits of the experimental data between 30 and 300 K to the Curie–Weiss law, leading to C = 3.814 cm^3 K mol^{-1} and θ = −13.24 K.

Conductivity measurement performed on a compressed pellet at room temperature gives a conductivity of ≈2×10^{-7} S.cm^{-1} indicative of an insulating behavior, as anticipated from the 1:1 stoichiometry and strong dimerization of the radical cations.

3.6. Pancake Interactions

The very specific, localized, short Se•••Se intermolecular contact found in the $FeCl_4^-$ salt between two $\mathbf{1}^{+\bullet}$ radical cations deserves some comments. First of all, this kind of association of radical cations is unknown in the chemistry of naphthalene/tetracene tetraselenides and diselenides as well as among tetrathia(selena)fulvalene salts. It is reminiscent, however, of several solid-state structures found, for example, in neutral dithiadiazolyl (DTDA) or diselenadiazolyl (DSDA) neutral radicals [49], where the individual radicals have a high tendency towards dimerization as a result of 'pancake bonding' interactions [50,51], a specific e^-–e^- pairing, where the radicals face each other. Such pairwise association of the DTDA/DSDA radicals by overlap of their SOMOs can occur in different ways, as shown in Scheme 4. Of these, by far the most common is the *cis*-cofacial mode, which involves the direct superposition of two radicals separated by a pair of S•••S [52] (or Se---Se) contacts [53]. The opposite situation of head-to-tail overlap is described as *trans*-cofacial while an intermediate one, only reported in DTDAs and associated with one single S•••S contact, is described as twisted-cofacial. Within the few reported examples of *cis*-cofacial diselenadiazolyl (DSDA) radicals [54–57], the Se•••Se distances between the facing radicals are found in the range 3.13–3.44 Å with an averaged value (calculated over 24 Se•••Se distances) of 3.23 Å. In that respect, the Se•••Se distance found here in (**1**)$FeCl_4$ at 3.197(2) is particularly short.

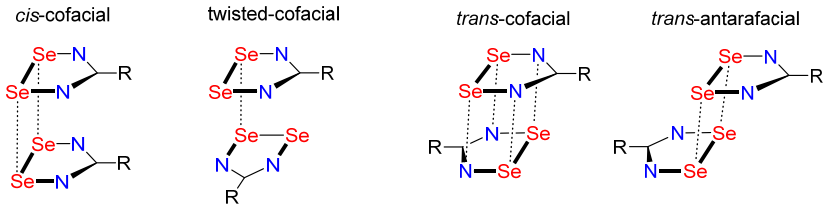

Scheme 4. Details of the most common solid-state association of diselenadiazolyl (DSDA) radicals.

Its consequence on the overlap pattern between the SOMO of the two radicals can be found in Figure 8a where the bonding combination of the two SOMOs has been drawn with a cut-off of 0.04 (left) and 0.03 (right). A similar analysis with the head-to-tail, *trans*-cofacial overlap found in (**1**)$_2$(Fe_2Cl_6O) is shown in Figure 8b, demonstrating the predominant localization of the bonding in the former twisted-cofacial arrangement. In both situations, the BSSE-corrected complexation energy is high, 37 kcal mol^{-1} in the twisted cofacial geometry and 34 kcal mol^{-1} in the *trans*-cofacial geometry. Those values unambiguously demonstrate that the dicationic species is strongly stabilized and indeed does not contribute to the magnetic response of the two salts.

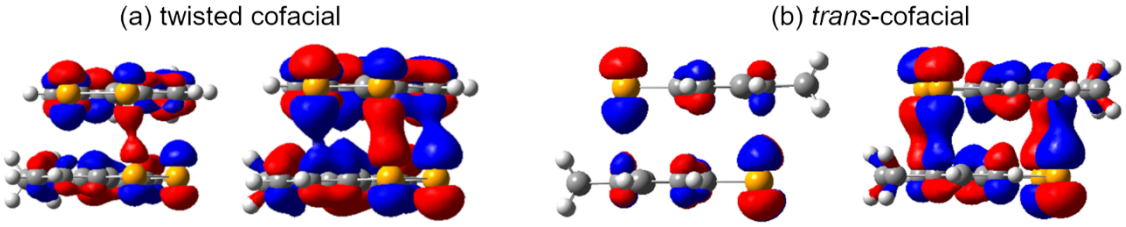

Figure 8. Representation of the HOMO of the dicationic (**1**)$_2^{2+}$ species, built out of the bonding combination of the individual SOMOs in (**a**) the twisted-cofacial arrangement of (**1**)$FeCl_4$ and (**b**) the *trans*-cofacial arrangement of (**1**)$_2$(Fe_2Cl_6O). For each geometry, the representation is given at 0.04 (left) and 0.03 (right) isovalues.

4. Conclusions

We have demonstrated here that naphthalene diselenide such as the acenaphthene diselenide **1** could be readily oxidized and isolated in cation radical form. Two different salts were isolated, showing remarkably different solid-state association of the radicals into dimers, either in one-dimensional, alternated stacks with a head-to-tail (trans-cofacial) organization or in a rare twisted-cofacial structure with a very short Se•••Se distance. In both examples, strong and directional Se•••Cl chalcogen bond interactions take place, involving all three σ-holes around the diselenide bridge, a consequence of their charge activation upon $1e^-$ removal from the neutral **1** to its cation radical. Further work along these lines will concentrate on other counterions with Lewis base character, as well as on charge transfer complexes with organic e^- acceptors.

Supplementary Materials: The following supporting information can be downloaded at: https://www.mdpi.com/article/10.3390/cryst16090555/s1, Figure S1: Field dependence of magnetization for (**1**)$FeCl_4$ at 100K; Figure S2: Cyclic voltammetry of **1**; Figure S3: Projection view along *a* of the unit cell of **1**, showing the tetrameric, chalcogen-bonded motif; Figure S4: Experimental X-ray powder diagram of the sample of (**1**)FeCl4 used for magnetic measurements, together with the theoretical ones deduced from the single crystal-ray structures of (**1**)$FeCl_4$ and $(\mathbf{1})_2(Fe_2Cl_6O)$; Table S1: Crystallographic data; Table S2: Final optimized coordinates of neutral **1**; Table S3: Final optimized coordinates of cationic $\mathbf{1}^{+\bullet}$.

Author Contributions: Conceptualization and supervision, M.F. and I.-R.J.; synthesis and crystal growth, H.P.P. and N.Q.; X-ray crystallography, O.J.; writing—original draft preparation, M.F.; writing—review and editing, M.F. and I.-R.J.; funding acquisition, M.F. and I.-R.J. All authors have read and agreed to the published version of the manuscript.

Funding: This work received financial support under the EUR LUMOMAT project and the Investments for the Future program ANR-18-EURE-0012 for a PhD grant to H.P.P. Other supports include the DYSCORDE project ANR-20-CE29-0011-02, the Magneto-e project ANR-22-CE07-0050-01, and the CoordinSCFs project ANR-23-CE07-0029-03. This work was granted access to the HPC resources of TGCC/CEA/CINES/IDRIS under the allocation 2024 AD010814136R2 awarded by GENCI. I.-R.J. received funding from the University of Bordeaux, Research Program GPR Light (Idex Bordeaux), the Région Nouvelle Aquitaine and Quantum Matter Bordeaux.

Data Availability Statement: The data presented in this study are available upon request from the corresponding author. The CCDC numbers 2574025-2574027 contains the supplementary crystallographic data reported in this paper. These data can be obtained free of charge from the Cambridge Crystallographic Data Center via www.ccdc.cam.ac.uk/data_request/cif (accessed on 18 August 2026).

Acknowledgments: We thank CDIFX (ISCR) for access to single-crystal X-ray diffractometers.

Conflicts of Interest: The authors declare no conflicts of interest.

References

1. Pizzi, A.; Terraneo, G.; Iacono, C.L.; Beccaria, R.; Dhaka, A.; Resnati, G. Taxonomy of Chemical Bondings: Opportunities and Challenges. *Angew. Chem. Int. Ed.* **2025**, *64*, e20250652. [CrossRef]
2. Fourmigué, M.; Lieffrig, J. Organizing radical species in the solid state with halogen bonding. *Top. Curr. Chem.* **2015**, *359*, 91–114. [CrossRef]
3. Fourmigué, M. Organic p-Radicals in the Solid State: From Localized to Delocalized s-Bonding. In *The Importance of Pi-interactions in Crystal Engineering*; Tiekink, E.R.T., Zukerman-Schpector, J., Eds.; John Wiley & Sons, Ltd.: Hoboken, NJ, USA, 2012; Chapter 6, pp. 143–162.
4. Kertesz, M. Pancake Bonding: An Unusual Pi-Stacking Interaction. *Chem. Eur. J.* **2019**, *25*, 400–416. [CrossRef]
5. Haberhauer, G.; Gleiter, R. Double Pancake Versus Long Chalcogen–Chalcogen Bonds in Six-Membered C,N,S-Heterocycles. *Chem. Eur. J.* **2016**, *22*, 8646–8653. [CrossRef]

6. Brown, J.T.; Zeller, M.; Rosokha, S.V. Effects of structural variations on π-dimer formation: Long-distance multicenter bonding of cation-radicals of tetrathiafulvalene analogues. *Phys. Chem. Chem. Phys.* **2020**, *22*, 25054–25065. [CrossRef]
7. Molčanov, K.; Milašinović, V.; Kojić-Prodić, B. Contribution of Different Crystal Packing Forces in π-Stacking: From Noncovalent to Covalent Multicentric Bonding. *Cryst. Growth Des.* **2019**, *19*, 5967–5980. [CrossRef]
8. Jérome, D. Organics Conductors: From Charge Density Wave TTF–TCNQ to Superconducting $(TMTSF)_2PF_6$. *Chem. Rev.* **2004**, *104*, 5565–5591. [CrossRef]
9. Imakubo, T.; Sawa, H.; Kato, R. Novel radical cation salts of organic π-donors containing iodine atom(s): The first application of strong intermolecular I···X (X = CN, halogen atom) interaction to molecular conductors. *Synth. Met.* **1995**, *73*, 117–122. [CrossRef]
10. Fourmigué, M.; Batail, P. Activation of Hydrogen- and Halogen-Bonding in Tetrathiafulvalene-Based Crystalline Molecular Conductors. *Chem. Rev.* **2004**, *104*, 5379–5418. [CrossRef]
11. Oliveira, R.; Groni, S.; Vacher, A.; Barrière, F.; Lorcy, D.; Fourmigué, M.; Maisonhaute, E.; Schöllhorn, B.; Fave, C. Electrochemical activation of TTF-based XB donors. A powerful, sensitive and selective analytical tool for probing halogen bonding in complex media. *Chem. Sel.* **2018**, *3*, 8874–8880. [CrossRef]
12. Oliveira, R.; Groni, S.; Fave, C.; Branca, M.; Mavré, F.; Lorcy, D.; Fourmigué, M.; Schöllhorn, B. Electrochemical Activation of a Tetrathiafulvalene Halogen Bond Donor in Solution. *Phys. Chem. Chem. Phys.* **2016**, *18*, 15867–15873. [CrossRef]
13. Beau, M.; Jeon, I.-R.; Jeannin, O.; Guizouarn, T.; Fourmigué, M. Activation of chalcogen bonding in tetrathiafulvalene derivatives with Se/S differentiation. *New J. Chem.* **2025**, *49*, 11501–11508. [CrossRef]
14. Beau, M.; Lee, S.; Jeannin, O.; Fourmigué, M.; Jeon, I.-R. Activating both halogen and chalcogen bonding interactions in cation radical salts of iodinated TTFs. *ChemPlusChem* **2020**, *85*, 2136–2142. [CrossRef]
15. Bevan, H.; Le Gal, Y.; Roisnel, T.; Jeannin, O.; Jeon, I.-R.; Fourmigué, M.; Lorcy, D. Charge Activation of Chalcogen Bonding Interactions in a Bis(Selenomethyl)-Substituted Tetrathiafulvalene and its Salts. *CrystEngComm* 2026, *in press*. [CrossRef]
16. Acampora, L.A.; Elman, B.S.; Sandman, D.J.; Jansen, S.; Jones, M.T.; Rataiczak, R.D.; Foxman, B.M. Structural and magnetic studies of electrochemically crystallized halides of 1,4,5,8-tetraselenonaphthalene (TSeN). *Inorg. Chem.* **1989**, *28*, 1579–1582. [CrossRef]
17. Shibaeva, R.P. *Extended Linear Chain Compounds*; Miller, J.S., Ed.; Plenum Press: New York, NY, USA, 1982; Volume 2, pp. 435–467.
18. Takimiya, K.; Aso, Y.; Otsubo, T.; Ogura, F. Syntheses and Properties of Dimethyl and Tetramethyl Anthra [1,9-cd:4,10-c′d′]bis [1,2]dichalcogenoles and Their Charge-Transfer Complexes. *Bull. Chem. Soc. Jpn.* **1991**, *64*, 2091–2102. [CrossRef]
19. Politzer, P.; Murray, J.S.; Concha, M.C. Σ-hole bonding between like atoms; a fallacy of atomic charges. *J. Mol. Model.* **2008**, *14*, 659–665. [CrossRef]
20. Murray, J.S.; Resnati, G.; Politzer, P. Close contacts and noncovalent interactions in crystals. *Faraday Discuss.* **2017**, *203*, 113–130. [CrossRef]
21. Scilabra, P.; Murray, J.S.; Terraneo, G.; Resnati, G. Chalcogen Bonds in Crystals of Bis(*o*-anilinium)diselenide Salts. *Cryst. Growth Des.* **2019**, *19*, 1149–1154. [CrossRef]
22. Fourmigué, M.; Dhaka, A. Chalcogen bonding in crystalline diselenides and selenocyanates: From molecules of pharmaceutical interest to conducting materials. *Coord. Chem. Rev.* **2020**, *403*, 213084. [CrossRef]
23. Shukla, R.; Dhaka, A.; Aubert, E.; Vijayakumar-Syamala, V.; Jeannin, O.; Fourmigué, M.; Espinosa, M. Understanding Reactivity and Assembly of Dichalcogenides: Structural, Electrostatic Potential, and Topological Analyses of 3H-1,2-Benzodithiol-3-one and Selenium Analogs. *Cryst. Growth Des.* **2020**, *20*, 7704−7725. [CrossRef]
24. Press, D.J.; Back, T.G.; Sutherland, T.C. Charge transfer complexes of electron-rich naphthalene *peri*-dichalcogenides with TCNQ. *Tetrahedron Lett.* **2012**, *53*, 1603–1605. [CrossRef]
25. Padikkal, H.P.; Jeannin, O.; Rouzières, M.; Clérac, R.; Jeon, I.-R.; Fourmigué, M. Chalcogen bond activation in cation radical salts of naphthalene *peri*-diselenides with S = 5/2 magnetic anions. *Dalton Trans.* **2026**, *55*, 5511–5518. [CrossRef]
26. Nietfeld, J.P.; Schwiderski, R.L.; Gonnella, T.P.; Rasmussen, S.C. Structural Effects on the Electronic Properties of Extended Fused-Ring Thieno [3,4-b]pyrazine Analogues. *J. Org. Chem.* **2011**, *76*, 6383–6388. [CrossRef]
27. Benson, C.G.M.; Schofield, C.M.; Randall, R.A.M.; Wakefield, L.; Knight, F.R.; Slawin, A.M.Z.; Woollins, J.D. Platinum Complexes of 5,6-Dihydroacenaphtho [5,6-cd]-1,2-dichalcogenoles. *Eur. J. Inorg. Chem.* **2013**, *3*, 427–437.
28. Sheldrick, G.M. SHELXT—Integrated space-group and crystal structure determination. *Acta Cryst.* **2015**, *A71*, 3–8. [CrossRef]
29. Sheldrick, G.M. Crystal Structure Refinement with SHELXL. *Acta Cryst.* **2015**, *C71*, 3–8. [CrossRef] [PubMed]
30. Farrugia, L.J. WinGX and ORTEP for Windows: An update. *J. Appl. Cryst.* **2012**, *45*, 849–854. [CrossRef]
31. Hohenberg, P.; Kohn, W. Inhomogeneous Electron Gas. *Phys. Rev. B* **1964**, *136*, 864–871. [CrossRef]
32. Parr, R.G.; Yang, W. *Density-Functional Theory of Atoms and Molecules*; Oxford University Press: New York, NY, USA; Oxford, UK, 1989.
33. Becke, A.D. A new mixing of Hartree–Fock and local density-functional theories. *J. Phys. Chem.* **1993**, *98*, 1372–1377. [CrossRef]
34. Becke, A.D. Density-Functional Thermochemistry. III. The Role of Exact Exchange. *J. Phys. Chem.* **1993**, *98*, 5648–5652. [CrossRef]

35. Lee, C.; Yang, W.; Parr, R.G. Development of the Colle-Salvetti correlation-energy formula into a functional of the electron density. *Phys. Rev. B* **1988**, *37*, 785–789. [CrossRef] [PubMed]
36. Frisch, M.J.; Trucks, G.; Schlegel, H.B.; Scuseria, G.E.; Robb, M.A.; Cheeseman, J.R.; Scalmani, G.; Barone, V.; Mennucci, B.; Petersson, G.A.; et al. *Gaussian 09, Revision B.01*; Gaussian, Inc.: Wallingford, CT, USA, 2010.
37. Grimme, S.; Antony, J.; Ehrlich, S.; Krieg, H. A consistent and accurate ab initio parametrization of density functional dispersion correction (DFT-D) for the 94 elements H-Pu. *J. Chem. Phys.* **2010**, *132*, 154104. [PubMed]
38. Lu, T.; Chen, F. Multiwfn: A multifunctional wavefunction analyze. *J. Comput. Chem.* **2012**, *33*, 580–592. [CrossRef] [PubMed]
39. Lu, T. A comprehensive electron wavefunction analysis toolbox for chemists. *Multiwfn. J. Chem. Phys.* **2024**, *161*, 082503. [CrossRef]
40. Aso, Y.; Yui, K.; Miyoshi, T.; Otsubo, T.; Ogura, F.; Tanaka, J. Dichalcogen-Bridged Acenaphthenes as New Electron Donors. *Bull. Chem. Soc. Jpn.* **1988**, *61*, 2013–2018. [CrossRef]
41. Batail, P.; Boubekeur, K.; Fourmigué, M.; Gabriel, J.-C.P. Electrocrystallization, an Invaluable Tool for the Construction of Ordered, Electroactive Molecular Solids. *Chem. Mater.* **1998**, *10*, 3005–3015. [CrossRef]
42. Ameerunisha, S.; Schneider, J.; Meyer, T.; Zacharias, P.S.; Bill, E.; Henkel, G. Synthesis and structural characterisation of Fe(II) and Cu(I) complexes of a new tetrafunctional N-donor ligand with dodecahedral or tetrahedral binding domains. *Chem. Commun.* **2000**, 2155–2156. [CrossRef]
43. Haselhorst, G.; Wieghardt, K.; Keller, S.; Schrader, B. The (m-oxo) bis [trichloroferrate (III)] dianion revisited. *Inorg. Chem.* **1993**, *32*, 520–525. [CrossRef]
44. Lledos, A.; Moreno-Manas, M.; Sodupe, M.; Vallriberra, A.; Mata, I.; Martinez, B.; Molins, E. Bent and Linear Forms of the (μ-Oxo)bis[trichloroferrate(III)] Dianion: An Intermolecular Effect—Structural, Electronic and Magnetic Properties. *Eur. J. Inorg. Chem.* **2003**, 4187–4194. [CrossRef]
45. Do, Y.; Simhon, E.D.; Holm, R.H. Improved syntheses of tetrachlorodi-.mu.-sulfidodiferrate(2–) ($[Fe_2S_2Cl_4]^{2-}$) and hexachloro-.mu.-oxodiferrate(2–) ($[Fe_2OCl_6]^{2-}$) and oxo/sulfido ligand substitution by use of silylsulfide reagents. *Inorg. Chem.* **1983**, *22*, 3809–3812. [CrossRef]
46. Koike, T.; Yokota, S.; Fujiwara, H.; Sugimoto, T.; Noguchi, S.; de Caro, D.; Valade, L. $FeOCl_6^{2-}$ Salt Formed by Electrochemical Oxidation of Ethylenedioxy-tetrathiafulvalenoquinone-1,3-dithiolemethide in the Presence of $FeCl_4^-$ Ion with a Silicon Wafer Electrode. *Inorg. Chem.* **2008**, *47*, 7074–7076.
47. Schmidbaur, H.; Zybill, C.E.; Neugebauer, D. Oxidative Coupling of the Selenolate Functions in $(C_6H_5)_3PC(Se)P(C_6H_5)_3$: Crystal Structure of $([(C_6H_5)_3P]_2CSe)_2^{2+}$, $Fe_2OCl_6^{2-}$ 4 CH_2Cl_2 Containing a Linear Fe-O-Fe Axis. *Angew. Chem. Int. Ed. Engl.* **1983**, *22*, 156–157.
48. Dehnicke, K.; Prinz, H.; Massa, W.; Pebler, J.; Schmidt, R. Die Reaktion von Trichlornitromethan mit Eisencarbonylen Kristallstruktur von $(PPh_4)_2[Fe_2OCl_6]$•2 CH_2Cl_2. *Z. Anorg. Allg. Chem.* **1983**, *499*, 20–30. [CrossRef]
49. Beer, L.; Cordes, A.W.; Myles, D.J.T.; Oakley, R.T.; Taylor, N.J. 1,2,3,5-Dithiadiazolyls and 1,2,3,5-diselenadiazolyls; stacking and packing of π-dimers. *CrystEngComm* **2000**, *2*, 109–114. [CrossRef]
50. Preuss, K.E. Pancake bonds: π-Stacked dimers of organic and light-atom radicals. *Polyhedron* **2014**, *79*, 1–15. [CrossRef]
51. Beneberu, H.Z.; Tian, Y.-H.; Kertesz, M. Bonds or not bonds? Pancake bonding in 1,2,3,5-dithiadiazolyl and 1,2,3,5-diselenadiazolyl radical dimers and their derivatives. *Phys. Chem. Chem. Phys.* **2012**, *14*, 10713–10725. [CrossRef]
52. Gleiter, R.; Haberhauer, G. Electron-rich two-, three- and four-center bonds between chalcogens—New prospects for old molecules. *Coord. Chem. Rev.* **2017**, *344*, 263–298. [CrossRef]
53. Beekman, R.A.; Boeré, R.T.; Moock, K.H.; Parvez, M. Synthesis, electrochemistry, structure and magnetic susceptibility of 5-*tert*-butyl-1,3-bis-(1,2,3,5-dithiadiazolyl)benzene. Structural effects of the bulky substituent. *Can. J. Chem.* **1998**, *76*, 85–93. [CrossRef]
54. Boere, R.T.; Hill, N.D.D. High Z′ structures of 1,2,3,5-dithiadiazolyls and of 1,2,3,5-diselenadiazolyls containing the first structurally characterized monomeric diselenadiazolyls. *CrystEngComm* **2017**, *19*, 3698–3707. [CrossRef]
55. Nascimento, M.A.; Heyer, E.; Clarke, J.J.; Cowley, H.J.; Alberola, A.; Stephaniuk, N.; Rawson, J.M. On the Design of Radical–Radical Cocrystals. *Angew. Chem. Int. Ed.* **2019**, *58*, 1371–1375. [CrossRef]
56. Taponen, A.I.; Wong, J.W.L.; Lekin, K.; Assoud, A.; Robertson, C.M.; Lahtinen, M.; Clérac, R.; Tuononen, H.M.; Mailman, A.; Oakley, R.T. Non-Innocent Base Properties of 3- and 4-Pyridyl-dithia- and Diselenadiazolyl Radicals: The Effect of N-Methylation. *Inorg. Chem.* **2018**, *57*, 13901–13911. [CrossRef]
57. Britten, J.F.; Clements, O.P.; Cordes, A.W.; Haddon, R.C.; Oakley, R.T.; Richardson, J.F. Stacking Efficiency of Diselenadiazolyl π-Dimers. Consequences for Electronic Structure and Transport Properties. *Inorg. Chem.* **2001**, *40*, 6820–6824. [CrossRef]

Disclaimer/Publisher's Note: The statements, opinions and data contained in all publications are solely those of the individual author(s) and contributor(s) and not of MDPI and/or the editor(s). MDPI and/or the editor(s) disclaim responsibility for any injury to people or property resulting from any ideas, methods, instructions or products referred to in the content.